ELSEVIER

Journal of Nuclear Materials 251 (1997) 98–106

journal of nuclear materials

Behavior and computer simulation of SiC under irradiation with energetic particles

J.M. Perlado *

Instituto de Fusíon Nuclear, E.T.S.I.I., Universidad Politécnica de Madrid, J. Gutierrez Abascal, 2, 28006 Madrid, Spain

Abstract

This paper reviews previous works focused on fundamental neutron damage simulations in β-SiC. The reason to propose ceramic composites based on SiC, instead of the monolithic form, is concluded, and the effect of radiation (neutron irradiation) on the macroscopic responses of the material are shown. Molecular dynamics simulations of threshold displacement energy, defect energetics, melting point, and 3–5 keV cascades are presented, together with a criticism of various interatomic potentials such as Pearson, Tersoff, and Modified Embedded Atom Model. Most of the presented results have been performed with Tersoff's potential which has demonstrated a better physics description of the material's parameters. The directional dependence of the threshold energy is mentioned, and the consequences of energetic cascades such as potential amorphization are compared with results of Si. The effect of the accumulation of damage, at a rate higher than expected in real Inertial Confinement Fusion applications is also mentioned. © 1997 Elsevier Science B.V.

1. Introduction

The use of SiC has a long history in nuclear power systems from being successful particle fuel coatings (TRISO, TRIple ISOtropic coatings) for high temperature gas cooled reactors (HTGR), and base material for temperature monitors in nuclear reactors. It has also been proposed for nuclear fusion from the 1970s. However, some of its properties, brittleness and high sensitivity to develop cracks, makes it a highly risky material for nuclear safety. More recently, interest has been shown in SiC fibers for the C matrix for high heat flux components, and in metal matrices (Al, Ti) for some potential structural applications. From the use of monolithic β-SiC, the present technology in fusion is proposing to solve those problems using SiC/SiC composites, which have some very interesting and critical properties: low activation, low afterheat, high temperature strength, and low electrical conductivity.

The low activation characteristic under neutron irradiation of SiC has been demonstrated for different environments, considering recycling, waste disposal, and atmospheric releases. However, careful analyses need to be done in any particular case considering the level of impurities, type of neutron spectrum, and irradiation time, to fully assess the appropriate frame for using the material. Different conceptual reactors in Magnetic Fusion (MFE), such as ARIES [1], TAURO [2], and Inertial Fusion (IFE), KOYO [3], HIBALL-II [4], have included the SiC in different forms as structural material for blanket systems.

There is an important need therefore to establish the effect of the radiation damage (neutron damage) in β-SiC and its composites leading to the modification of properties such as: hermeticity, electrical conductivity, chemical compatibility with coolant/blanket, dimensional stability, and mechanical properties, and also to investigate the microscopic mechanisms which guide those effects. In addition to some starting experimental programs, related to nuclear fusion activities, to qualify the SiC/SiC composites, there is an increasing need of computational simulations of the basic physics of radiation damage in β-SiC, and clear understanding of the dynamics of defects generation and transport in this covalent material.

Calculations on β-SiC, using molecular dynamics, describing high energy cascades formation, threshold displacement energy and melting point will be presented. Moreover, a preliminary analysis of accumulated radiation

* Tel.: +34-1 336 3108; fax: +34-1 336 3002; e-mail: mperlado@denim.upm.es.

PII S0022-3115(97)00258-4

damage, relevant for IFE reactors with materials under a short and intense pulse of neutrons, is given.

Different interatomic potentials have been proposed in the past to model covalent material such as SiC; in particular for this material, Tersoff [5], Pearson [6], and Modified Embedded Atom Model (MEAM) [7], have been considered and compared [8,9] using defect energetics results. The Tersoff potential has been used in our model incorporated in the computer code MOLDYCASK [10–12], because it is demonstrated to have better agreement with the available experimental results.

2. Low-activation material

It was shown that SiC irradiated up to 30 years in a 'soft' neutron environment with an average energy of $\langle E \rangle = 0.1$ MeV and a total flux of $\approx 10^{15}$ n cm^{-2} s^{-1}, such as in IFE reactors, has a very good performance considering recycling options (hands-on, remote) and disposal (Shallow Land Burial, SLB) [13,14]. When considering a 'hard' neutron spectrum, $\langle E \rangle = 2.1$ MeV, with a total flux of $\approx 2 \times 10^{15}$ n cm^{-2} s^{-1} and an irradiation time of 2.5 years, the limitations in the environmental behavior are clearly observed in these cases, and they could impose more restrictive conditions of operations. The reason for the large increase of the surface gamma dose rate is the formation of the γ emissor ^{26}Al ($T_{1/2} = 7.2 \times 10^5$ y) from ^{28}Si through nuclear reactions

$$^{28}\mathrm{Si(n, np)}^{27}\mathrm{Al(n, 2n)}^{26}\mathrm{Al}; \qquad ^{28}\mathrm{Si(n, d)}^{27}\mathrm{Al(n, 2n)}^{26}\mathrm{Al},$$

which both include reactions with a threshold close to 14 MeV. The content of impurities is not significant in the long-term in the hard spectrum because the maximum contributor to the effect in that range is the Si, which is the major component. However, remote recycling at 50 years is also limited by ^{60}Co from impurities. That effect is observed in the calculation of neutron activation corresponding to porous SiC tubes components of the blanket of the IFE reactor KOYO irradiated 2 years under a hard neutron spectrum corresponding to the first rows of the blanket receiving the $\langle E \rangle \approx 12$ MeV neutron burst from the target [15], and also the effect of ^{24}Na (1 day) and ^{46}Sc (1 month–1 year) is shown in a reduced range. In the case of soft neutron spectrum the contribution of some impurities becomes important in recycling, and it can introduce a significant difference with the case of pure SiC. For SLB considerations the effect is also critical for hard spectrum because of the influence of ^{26}Al, and it needs to be considered also for the soft spectrum because of the effect of some impurities such as Nb and N, which must be strictly controlled.

Related to accidental releases simulations [16], SiC (pure and with impurities) fulfills the current evaluation criteria in both situations of hard and soft neutron spectra with larger values for the hard spectrum because of the formation of ^{24}Na from ^{28}Si through threshold chain reactions [16]. The difference between pure and with impurities content is larger for shorter irradiation times, and the effect of irradiated SiC/SiC, which has a maximum after 1 year of irradiation (0.5 mSv kg^{-1}) which is seven times larger than that after 30 years of irradiation, is remarkable; this effect is due to impurities Bi (producing ^{210}Po), Tb (producing ^{160}Tb), and W (producing ^{192}Ir).

3. Properties and irradiation effects in SiC and composites

A brief resume of macroscopic properties which justify the interest on these materials is given, together with the effect of radiation damage on them. There are other papers on this specific subject [17–21].

3.1. Macroscopic responses

In principle, the resistance of ceramic materials is enlarged because the stress is transmitted from the matrix to the fibers which have a larger resistance. The values of the resistance to fracture in composites with a ceramic matrix are very high because they absorb energy when fibers are extracted from the matrix provoking the deflection of cracks and their final stop.

The hydrogen in high density SiC, produced by chemical vapor deposition (CVD), has very low diffusion coefficients, but composites produced with the same techniques have a porosity of 10–15%. In conditions of thermal shocks or changes in volume, SiC composites can have leakage of He, 10^{-6}–10^{-1} mol s^{-1}, which needs to be corrected for using that material under pressure through sealant layers of other ceramics and glasses.

In oxidant atmosphere, SiC forms a dense film of SiO_2 apparently auto-sealant. At O_2 pressures lower than 10^{-8} atm and temperatures lower than 900°C the active oxidation of SiC starts. SiC is decomposed in the presence of pure H, but it is inert in the presence of an atmosphere of H_2, N_2. The main reactions between SiC and liquid metals are those which result from the interchange of C. There is evidence of corrosion in contact with liquid lithium at temperatures higher than 600°C. However, experiments with $Li_{17}Pb_{83}$ show a good stability at 800°C during 1500 h.

The characteristics under thermal shock of the monolithic and composites SiC are very different, and it was concluded that composites behave fairly good under these situations. For almost similar conditions, at 1500°C/s, monolithic samples failed in 1.5 cycle in average, but composites needed 25. SiC composites show that they can tolerate an important damage in the matrix without loss of the maximum failure or fracture stress, with a low speed of crack propagation explained by the presence of 'bridges' due to the fibers.

3.2. Irradiation effects

Bulk silicon carbides exhibit a phenomena called 'lattice swelling' between 60 and 1000°C, which is the result of volume changes because of the introduction of defects and chemical disorder. Above 1000°C there is void swelling similar to metals. The lattice expansion saturates at a few tenths of a dpa and afterwards is independent of the fluence up to 40–60 dpa, with a final linear change of 1% at room temperature decreasing with temperature to 0.1% at 1000°C. The void swelling rate is considerable lower than in metals with $\Delta V/V = 0.2\%/\text{dpa}$.

The elastic modulus, the tensile and bend strengths of both bulk β-SiC and SiC fibers increase after irradiation.

Since heat in SiC is carried by phonons, irradiation produced defects can significantly reduce its thermal conductivity by scattering phonons. This reduction will be smaller at high temperatures. In SiC monocrystals of high purity, thermal conductivities up to 5000 W m^{-1} K^{-1} have been measured at 50 K, and 500 W m^{-1} K^{-1} at room temperature. The conductivity in the composites is very much reduced because their high porosity together with the large area of the matrix–fiber interface increases the phonon scattering and decreasing conductivity. However, 2D SiC/SiC composites are being developed increasing their conductivity to 73 W m^{-1} K^{-1}, approaching that of the monocrystal at 1000°C.

SiC is a semiconductor with typical electric resistivities at room temperature from $\rho = 1$ to 10 Ω cm, and insulators with values as high as 10^{13} Ω cm can be produced by doping with BeO to produce an insulating grain boundary phase. Neutron irradiation reduces the number of carriers and increases the resistivity by factors of 10 to 10 000.

4. Molecular dynamics model and interatomic potential

The molecular dynamics code (MOLDYCASK) [10–12] has been implemented on the massively parallel computer CRI T3D at Lawrence Livermore National Laboratory.

Huang et al. [8,9] have done an exhaustive comparison of three SiC potentials: Tersoff [5], Pearson [6] and modified EAM potential [7]. Their conclusion is that the Tersoff potential is rather appropriate for describing defect properties in SiC. In particular, it correctly describes the vacancy formation energies in both sublattices and predicts the fact that Si antisites are more difficult to create than C antisites, in good agreement with first principles calculations [22] (see Table 1).

The MOLDYCASK version on T3D is based on the PVM message passing library [23]. The code runs on 128 processors at a rate of 2 μs/atom/timestep when using the SW potential, and at a rate of 4 μs/atom/timestep when using the Tersoff potential, both with a cut-off between the first and second nearest neighbor shells. One MD iteration takes 2 to 4 s of the CPU for a crystal with 1 million atoms, depending on the potential. It solves the Tersoff potential [5] to describe interactions in SiC, and the Stillinger–Weber (SW) potential for silicon [24]. Periodic boundary conditions are used in the ⟨100⟩ and ⟨010⟩ directions, with a free surface at the topmost (001) plane. The bottom (001) plane is held fixed and a thermostat is implemented by coupling the atoms in the next four (001) planes to a thermal reservoir at constant temperature. Energy is prevented from re-entering the simulation box through the periodic boundaries by application of a damping layer in the atomic planes adjacent to the boundaries.

Table 1
Results of defect energetics in SiC [8,9]

Energies (eV)	Pearson et al. [6]	MEAM	Tersoff	First principles
$E^f(V_{Si})$	6.70	14.28	12.46	12.60
$E^f(V_C)$	5.26	9.58	11.61	11.70
$E^{d-m}(V_{Si})$	7.39	2.88	5.83	N/A
$E^{d-m}(V_C)$	6.10	5.24	8.94	N/A
$E^{i-m}(V_{Si})$	4.30	2.72	6.08	N/A
$E^{i-m}(V_C)$	0.50	2.61	3.48	N/A
$E^f(I_{Si\_}T_C)$	3.23	5.96	4.08	8.00
$E^f(I_{C\_}T_C)$	3.37	−3.07	2.29	4.40
$E^f(I_{Si\_}T_{Si})$	10.55	2.09	8.00	8.30
$E^f(I_{C\_}T_{Si})$	3.80	−3.04	0.23	1.90
$E^m(I_{Si})$	6.04	4.12	3.95	N/A
$E^m(I_C)$	1.47	1.29	3.58	N/A
E (Si antisite)	3.66	7.21	5.55	6.40
E (C antisite)	−3.33	2.17	0.61	0.20

5. Threshold displacement energy and melting point

For the studies of melting [10,12], simulation boxes, containing 384 atoms with free surfaces in the $+Z$ and $-Z$ directions and periodic boundaries elsewhere, with a Zinc-blende structure with an initial adaptive time of 0.75 fs and a high temperature lattice parameter of 4.425 Å, have been used. A broad melting transition has been located between 2500 and 3000 K, which is shown in Fig. 1 where the total energy of the system is plotted as a function of temperature. The latent heat of the transition is at ~ 0.5 eV/atom. The experimental melting point of SiC is 2818 K [25]. In Fig. 2, the Si–C paired distribution at various temperatures is shown.

The results of the threshold displacement energy calculations [10,12] are summarized in Table 2. A Zinc-blende structure was used including 1728 atoms, bulk surfaces, a low-temperature lattice parameter of 4.36 Å and an initial adaptive timestep of 0.25 fs. For Si primary knock on atoms (PKA) along the [001] direction, the threshold is found between 30 and 35 eV. Fig. 3a represents the x, y, and z displacement of the 30 eV Si recoil as a function of time. As can be clearly seen, the atom moves along [001]

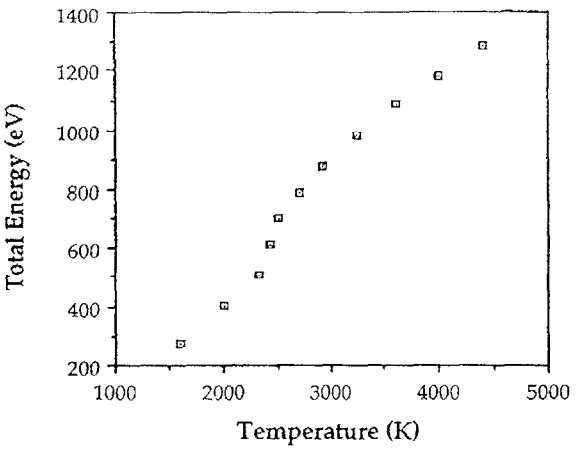

Fig. 1. Total energy of a SiC crystal versus temperature. The discontinuity indicates the phase transition range [10].

but falls back into its original position after ≈ 0.2 ps. For the rest of the simulation, the PKA simply fluctuates around its lattice site. In Fig. 3b the result for a 35 eV Si PKA is displayed. The z-coordinate of the PKA increases as the atom moves along [001]. In contrast to the previous case, at 35 eV the PKA remains stable at a distance $\sim 0.8a_0$ from its original position. Detailed analysis of the data after 2 ps shows that the PKA forms a [001] split interstitial with the atom originally in the replacement position. A vacancy is left at the PKA site. The distance between the atoms in the dumbbell is $0.5a_0$ Å. For C recoils along [001], the threshold energy for defect production was found to be between 35 and 40 eV. The resulting Frenkel pair was composed of a C–C split [001] dumbbell interstitial with the two atoms separated by $0.3a_0$, and a vacancy at the C PKA site.

Along [111], no defects were produced for Si recoils at $E_{\mathrm{pka}} \leq 30$ eV. At $E_{\mathrm{pka}} = 35$ eV, a C–C [110] split interstitial was found with a C vacancy at the first neighbor site to the Si PKA. Fig. 4 illustrates this case, and it is interesting

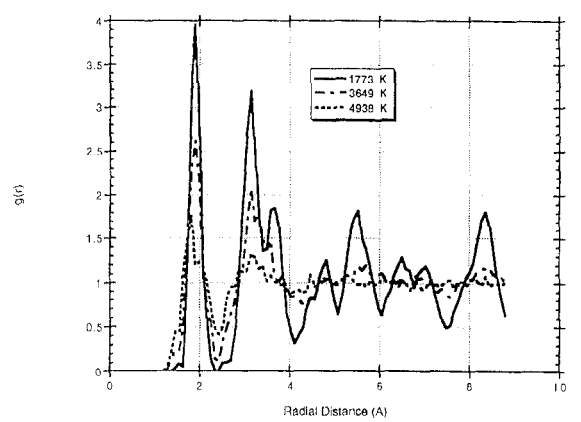

Fig. 2. Si–C P Pair distribution at various temperatures [12].

Table 2
Threshold energies for defect production on Si and C sublattices of β-SiC vs. crystallographic directions [10]

Defect threshold energies		
Direction	PKA type	PKA energy (eV)
[001]	Si	35
	C	40
[111]	Si	25
	C	25
[110]	Si	80
	C	30
[111]	Si	40

to note that this event did not result in any net displacement of silicon atoms, but produces a Frenkel pair in the C sublattice. For C recoils, the threshold energy for defect production was between 20 and 25 eV, lower than for Si PKAs. This may be understood in terms of the crystal symmetry. Along [111], the symmetry for C recoils is different from that for Si. Here, the C PKA moves along the cube diagonal through the tetrahedral sit without encountering any atom directly in its path for a distance of $3\sqrt{3}/4a_0$. The situation can be reversed by simulating trajectories along $[-1, -1, -1]$; here a Si recoil moves a distance $3\sqrt{3}/4a_0$ without encountering an atom directly in its path, while a C PKA must displace its nearest neighbor Si atom towards the tetrahedral site in the unit cell. For Si recoils along [111] the threshold energy was found between 35 and 40 eV. For C PKAs, no stable defects were formed up to $E_{\mathrm{pka}} = 50$ eV.

The largest difference between Si and C recoils was found along the [110] direction. For Si PKAs, the threshold for defect production was found between 80 and 85 eV. At 80 eV, the defect formed by this recoil was a C–C split interstitial with a C vacancy at the first tetrahedral neighboring site to the Si PKA, and the Si PKA fell back to its original position. After a short annealing run at 500 K followed by quenching of the kinetic energy of crystal, this defect was observed to annihilate, indicating its metastable nature. At 85 eV, however, the event resulted in a Si–Si split interstitial with a Si vacancy at the original Si PKA site (Fig. 5). For C recoils along [110], a C–C split interstitial was found for C PKA energy of 30 eV. No defects were found at $E_{\mathrm{pka}} = 25$ eV. The very high value of E_{d} in the silicon sublattice along [110] is consistent with results for pure silicon [26].

6. High energy displacement cascades

A 5 keV recoil was started from above the free surface and came to rest in the lattice approximately 50 Å from the

surface. The box for these computations [11] contained 175616 atoms, and the side-length was 120 Å.

Fig. 6 shows the pair correlation functions in a region of disordered material before and after the cascade. The center of the region was chosen from a projection into two dimensions of the set of atoms with $E_p > 0.3$ eV. The regions are cubes with a side-length of 16 Å. To calculate $g(r)$, we apply periodic boundary conditions. Fig. 6a shows the full pair correlation function. Some broadening of the crystalline peaks is apparent after the cascade compared to the $g(r)$ from the perfect crystal at 300 K, but clearly, a large degree of crystallinity remains within this region. Obviously, no direct-impact amorphization results from cascades at these energies in SiC. Fig. 6b and c show the partial pair correlation functions for carbon and silicon atoms, respectively, and for this same event. Because the melting point of SiC is so high, the cascade lifetime, defined as the time during which the average cascade temperature remains above T_m, is extremely short and the system does not melt.

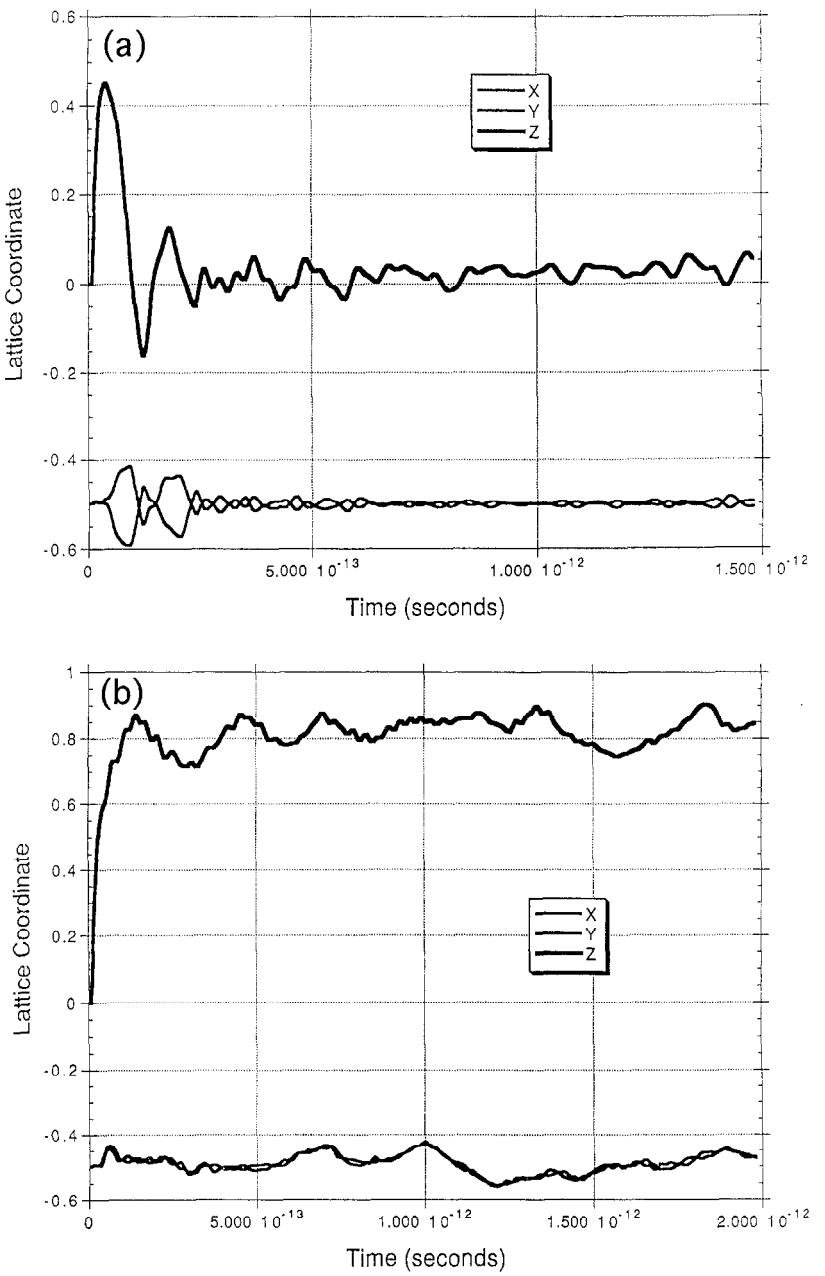

Fig. 3. Components of the displacement vector for: (a) 30 eV Si PKA along [001], (b) 35 eV Si PKA along [001] [10].

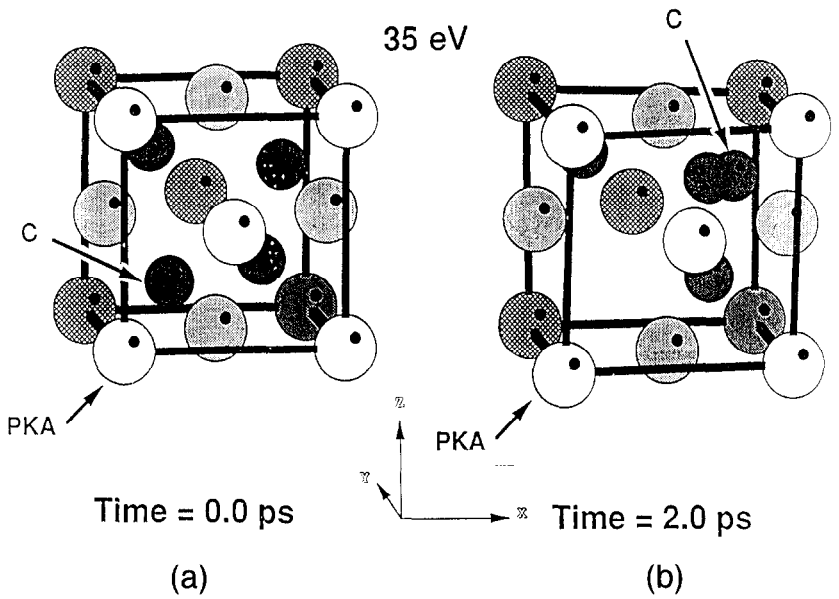

Fig. 4. Unit cell in which a 35 eV Si PKA along [111] is simulated (a) at $t = 0$, and (b) at the end of the event, $t = 2.0$ ps [10].

This is in direct contrast with the case of silicon, in which the cascade results in direct impact amorphization [26]. Fig. 7 shows the pair correlation function for the atoms in the disordered region at two times, at the time corresponding to the maximum extent of the cascade region, and after the system reaches thermal equilibrium with its surroundings. At 1.1 ps, the $g(r)$ resembles that of liquid silicon. After the rapid ($\approx 10^{14}$ K/s) resolidification process, the cascade region is left in the amorphous state, as shown by the $g(r)$ at 8 ps. The lifetime of the cascade, when defined as above, is close to 2 ps, that is, more than an order of magnitude larger than that for the SiC events.

Although these cascades do not result in direct amorphization of the SiC lattice, a number of displacements occurs in both the silicon and the carbon sublattices.

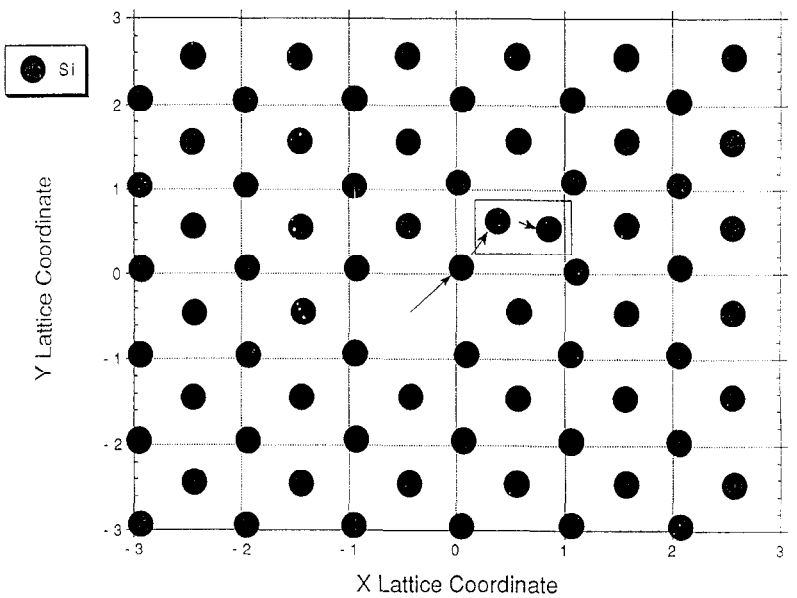

Fig. 5. X–Y sectional view of Si sublattice for 85 eV Si PKA along [110] after $t = 2.0$ ps [12].

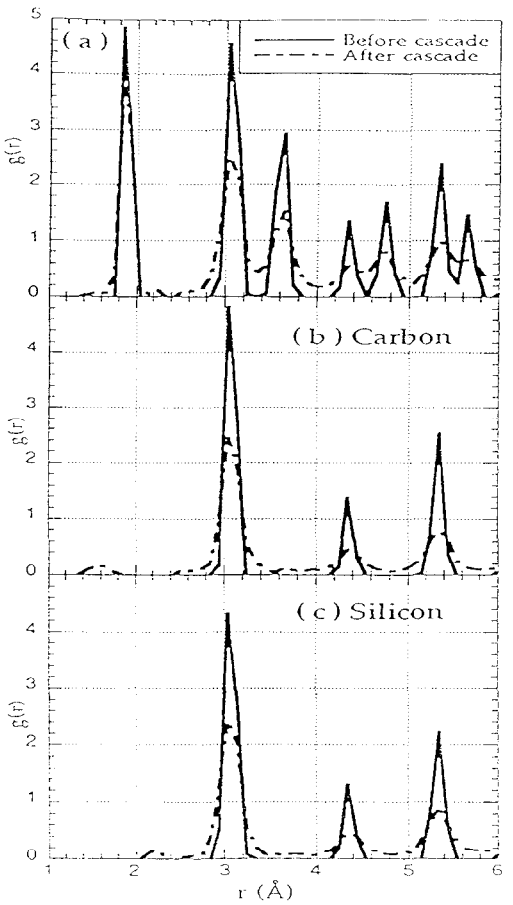

Fig. 6. Total pair correlation function in the SiC disordered region (a), and partials for C (b) and Si (c) atoms [11].

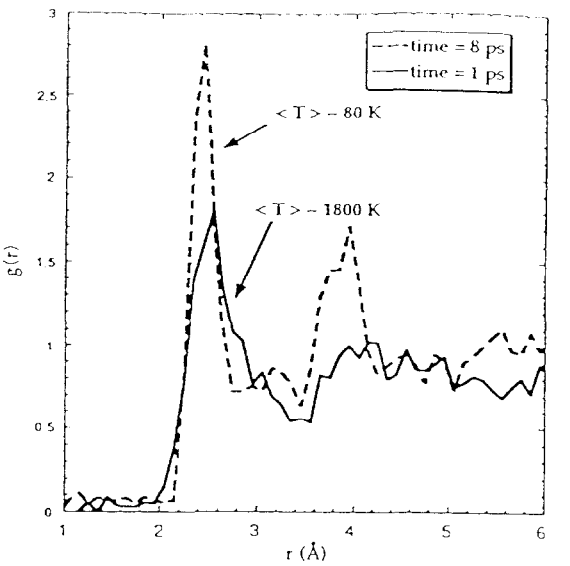

Fig. 7. Pair correlation function of Si at the maximum extent of the Si cascade (1 ps), and at equilibrium (8 ps).

During the evolution of a 5 keV cascade, it is noticed that although the number of replacements is nearly identical in both sublattices during the early stages of the cascade, nearly twice as many carbon atoms than silicon atoms are displaced after the first ps. Also interesting to note is that the total mean square displacement has a very small value of only $\Sigma r^2 = 1900$ Å^2, if we exclude the total distance traveled by the incident atom from the calculation. This corresponds to a mixing efficiency $Dt/\phi F_D \approx 1$ Å^5/eV. In contrast, for 5 keV cascades in silicon, the average value of Σr^2 is $\approx 20\,000$ Å^2, corresponding to $Dt/\phi F_D \approx 12$, about an order of magnitude larger than that for SiC. As mentioned above, the SiC cascades result in a larger number of displacements in the C-sublattice than in the Si-sublattice. Table 3 provides some of these data, together with those for overlap of 3 keV cascades in SiC at 300 and 1300 K. The vacant sites are defined as those modes in the crystal which have no atoms within half an atomic diameter of the site center. It is interesting to note that the number of vacancies in the carbon sublattice (N_V(C)) is always at least twice that in the silicon sublattice. Similarly, the number of atoms with potential energy in excess of 0.3 eV above the ground state is also double in the carbon sublattice. It is evident from these simulations that the overlap of cascades in SiC results in linear damage accumulation, irrespective of temperature. That is, the number of vacancies and the number of replacements doubles as the number of recoils doubles, even at 1300 K. This appears to indicate that the damage produced by the cascades in SiC is extremely stable, even at elevated temperatures. To further test this assumption, we continued

Table 3
Vacancy numbers for 3–5 keV cascades in SiC [11]

	5 keV, 300 K	3 keV, 300 K	2 × 3 keV, 300 K	3 keV, 1300 K	2 × 3 keV, 1300 K
N_v (total)	38	22	50	23	67
N_v (C)	26	15	37	16	47
N_v (Si)	12	7	13	7	20
N ($E_p > 0.3$ eV)	405	262	510	261	552
N_C	260	171	374	170	334
N_{Si}	145	90	180	94	177

to run one of the 3 keV cases at 1300 K that contained damage accumulated from two recoils. Even after 100 ps at 1300 K, the number of atoms with $E_p > 0.3$ eV had not changed. More simulations are needed in order to properly evaluate the thermal stability of the damage in SiC. Nevertheless the results seem to point toward high stability of damage at elevated temperatures in SiC.

7. Accumulated damage

Under Inertial Fusion conditions, it is expected that fluences as high as 30 dpa will be accumulated on the first wall over the lifetime of the reactor. More importantly, the dose will be accumulated in the form of neutron burst with approximately 0.1 dpa/burst. For a first wall 5 m away from the DT capsule, this leads to $\approx 2.5 \times 10^{14}$ n/cm^2 at the first wall. Since the duration of the pulse at the location of the wall is expected to be ≈ 1 μs, neutron fluxes as large as 10^{20} n/cm^{2}s are expected. These are enormous fluxes which may lead to cascade overlap effects that must be understood and taken into consideration. Moreover, operating conditions in the reactor are expected to be such that time intervals of 0.1 s at 1300 K will elapse in between pulses, and therefore must also be carefully understood.

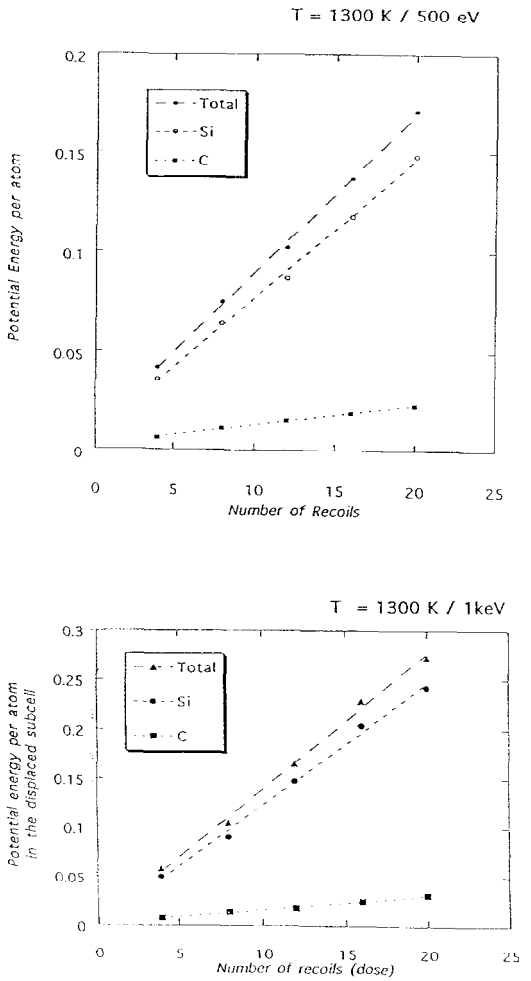

Fig. 8. Potential energy per atom in the displaced subcell versus number of recoils (dose) [11].

Damage accumulation simulations [11] were performed by accumulating 500 eV and 1 keV Si-recoil cascades in the same SiC crystal at 1300 K. Each recoil is followed for 3 ps, at which time the next recoil is introduced. For the conditions used, the simulated dose rate is $\approx 10^{25}$ cm^{-2} s^{-1}. The total accumulated dose is $\approx 2 \times 10^{14}$ recoils/cm^2. Although the simulated dose rate is larger than that expected in a reactor, the results should be indicative of the actual behavior of SiC, since, as we have shown above, even annealing a cascade for 100 ps does not lead to any morphology changes in the damage.

Fig. 8 shows the increase in potential energy per atom in the region of the displacement cascade versus dose for up to 20 (2×10^{14}) 500 eV (a) and 1 keV (b) Si recoils. The figure shows that damage accumulation is in fact linear over the complete dose range investigated, even at 1300 K. The results clearly show that no self-annealing of the cascade occurs in SiC, even at elevated temperatures, since otherwise, the temporal and spatial interaction between the cascades should lead to deviations from linearity.

Acknowledgements

This is an authentic compilation of previous works performed in collaboration with scientists from Lawrence Livermore National Laboratory (LLNL). I would like to especially acknowledge Dr T. Díaz de la Rubia (LLNL) for many discussions, for his introducing tutorial in this area, and continuing collaboration in new subjects, and Dr M.T. Tobin (LLNL) for his enthusiastic interest and support. In this work a large credit is due to Dr M.W. Guinan (LLNL) and Dr J. Wong. Working together with Professor J. Sanz and Dr A.S. Pérez, from my Institute, I got a better understanding of critical characteristics of SiC and its composites. Special thanks, here and now, to Professor G. Velarde, head of the Institute of Nuclear Fusion (UPM), for his continuous strong support, recognizing the importance of this subject for his dream of Inertial Fusion Energy.

References

[1] F. Najmabadi, R.W. Conn, Fusion Technol. 21 (1992) 1721.
[2] A.S. Pérez Ramírez et al., J. Nucl. Mater. 233–237 (1996) 1257.
[3] K. Mima et al., 15th Int. Conf. Plasma Phys. Contl. Nucl.

Fusion Re., Seville, Spain, 26 Sep.–1 Oct. 1994, IAEA-CN-60/F-I-5.
[4] B. Badger et al., HIBALL-II, An Improved Conceptual Heavy Ion Beam driven Fusion Reactor Study, KfK-3840, UWFDM-265, 1985.
[5] J. Tersoff, Phys. Rev. B39 (1989) 5566.
[6] E. Pearson et al., J. Cryst. Growth 70 (1984) 33.
[7] M.I. Baskes, Phys. Rev. B46 (1992) 2727.
[8] H. Huang, N. Ghoniem, J. Wong, M. Baskes, Mater. Sci. Eng. 3 (1995) 615.
[9] H. Huang, PhD thesis, Department of Nuclear Engineering, UCLA (1995).
[10] J. Wong, T. Díaz de la Rubia, M.W. Guinan, M. Tobin, J.M. Perlado, A.S. Pérez, J. Sanz, J. Nucl. Mater. 212–215 (1994) 143.
[11] T. Díaz de la Rubia, J.M. Perlado, M. Tobin, J. Nucl. Mater. 233–237 (1996) 1096.
[12] J. Wong, T. Díaz de la Rubia, M.W. Guinan, J.M. Perlado, Melting and Defect Production in SiC using the Tersoff Interatomic Potentials, in: OBES/OFE Workshop on SiC, Santa Barbara, Aug. 1993.
[13] J. Sanz, J.M. Perlado, A.S. Pérez, D. Guerra, J. Nucl. Mater. 191–194 (1992) 1450.
[14] J. Sanz, J.M. Perlado, D. Guerra, A.S. Pérez, Fusion Technol. 21 (1992) 2009.
[15] J.M. Perlado, K. Mima, S. Nakai, E. Alonso, E. Muñoz, J. Sanz, J. Nucl. Mater. 233–237 (1996) 1523.
[16] J. Sanz, A.S. Pérez, J.M. Perlado, M. Zucchetti, J. Nucl. Mater. 212–215 (1994) 673.
[17] M.W. Guinan, T. Díaz de la Rubia, LLNL Internal Report, Oct. 1991.
[18] A.S. Pérez, PhD thesis, Polytechnical University of Madrid (1995).
[19] S.J. Zinkle, C. Kinoshita, these Proceedings, p. 201.
[20] T. Suzuki, T. Yano, T. Mori, H. Miyazaki, T. Iseki, Fusion Technol. 27 (1995) 314.
[21] L.L. Snead, R.H. Jones, A. Kohyama, P. Fenici, J. Nucl. Mater. 233–237 (1996) 26.
[22] C. Wang, J. Bernholc, R. Davis, Phys. Rev. B38 (1988) 12752.
[23] PVM Message passing library.
[24] F.H. Stillinger, T.A. Weber, Phys. Rev. B31 (1985) 5262.
[25] T.B. Massalski et al., Binary Alloy Phase Diagrams, Vol. 1 (ASM International, Metals Park, OH, 1990).
[26] T. Díaz de la Rubia, G.H. Gilmer, Phys. Rev. Lett. 74 (13) (1995) 2507.